ELSEVIER

Chemical Engineering Science 60 (2005) 1477–1489

Chemical Engineering Science

www.elsevier.com/locate/ces

Modeling simultaneous biological clogging and physical plugging in trickle-bed bioreactors for wastewater treatment

Ion Iliuta*, Faïçal Larachi

Chemical Engineering Department, Laval University, Cite Universitaire, Qué., Canada G1K 7P4

Received 19 August 2004; received in revised form 28 September 2004; accepted 29 October 2004

Abstract

A major drawback limiting the use of trickle-bed bioreactors for biological wastewater treatment is ascribed to the concomitant *biological clogging* and *physical plugging* phenomena induced, respectively, by the formation of an excessive amount of biomass and the retention of inert suspended fine particles advected in the liquid influent stream. Biomass growth and fine particles deposition permanently reshape the bed pore structure and narrow the free interstitial space left to the fluids flow thus occasioning progressive bed obstruction often accompanied with pressure drop build-up for the cocurrent gas–liquid flows taking place in trickle-bed biofilters. In these circumstances, for maintaining acceptable operating cycles, the unit must be backwashed and/or shutdown regularly for removing the excess biomass and for cleaning from the specific solid deposit. A predictive two-dimensional dynamic model linking the two-phase flow hydrodynamics to the space-time distribution of bioclogging/biokinetics and of inert fine particles deposition via deep-bed filtration in trickle-bed bioreactors for wastewater treatment was developed. The model was based on the volume-average mass and momentum balance equations for the gas and liquid phases and continuity equation for the solid phase, the volume-average species balance for the fine particles, simultaneous transport and consumption of substrate (pollutant) and oxygen within the biofilm and collecting solid particle, and the volume-average species balance equations in the liquid and gas phases. Phenol biodegradation by *Pseudomonas putida* as the predominant species immobilized on activated carbon was chosen as a case study to illustrate the incidence of biomass accumulation on trickle-bed bioreactor hydrodynamics.

Keywords: Trickle bed reactors; Biological clogging; Physical plugging; Mathematical modeling

1. Introduction

Biological wastewater treatment is a widely accepted remedy that has been extensively and successfully adapted to deal with a broad spectrum of domestic/residential, agricultural, mining and industrial commercial applications. Since pollutant degradation occurs at normal temperature and pressure, biological wastewater treatment represents a proven energy-efficient technology when compared to alternative energy-demanding physical and chemical abatement processes (e.g., catalytic oxidation, incineration, advanced oxidation processes, scrubbing, regenerative adsorption, etc.). Biodegradation is a low operating and maintenance cost option and is attractive because it offers the possibility of complete mineralization of the polluting agents.

The two main types of bioreactors utilized in biological wastewater treatment are activated sludge processes and fixed-bed bioreactors. While in traditional activated sludge treatment, microorganisms are suspended in the liquid, they are immobilized on a stationary solid surface in fixed-bed bioreactors. The oldest form of fixed-bed bioreactors is the so-called trickle-bed bioreactor that has been utilized since the 19th century (Benthack et al., 2001). But it has only been during the past few decades that fixed-bed bioreactors have gained renewed interest (Chaudhry and Bed, 1998; Benthack et al., 2001), compared with the activated sludge process, due to their smaller reactor size, improved removal

* Corresponding author. Tel.: +1 4186562131X4790; fax: +1 4186565993.
E-mail addresses: ion.iliuta@gch.ulaval.ca (I. Iliuta), faical.larachi@gch.ulaval.ca (F. Larachi).

0009-2509/$ - see front matter © 2004 Elsevier Ltd. All rights reserved.
doi:10.1016/j.ces.2004.10.016

efficiency, reduced odor annoyance, and robustness toward hydrodynamic variations and toxic shocks in feed concentration. Another troublesome feature is the filtration of suspended particles that enables operation of fixed-bed bioreactor units with no downstream clarifiers (Jacob et al., 1996, 1997), an intrinsically embodied part of an activated sludge process. As a result, fixed-bed bioreactors have emerged as an alternative to traditional activated sludge secondary treatment and as complementary tertiary treatment step downstream of an activated sludge process (Pujol et al., 1992).

A major disadvantage limiting the use of trickle-bed bioreactors for biological wastewater treatments is attributed to the progressive simultaneous *biological clogging* and *physical plugging* phenomena induced by the formation of an excessive amount of biomass (van Lith et al., 1994; Weber and Hartmans, 1994; Sorial et al., 1995; Weber and Hartmans, 1996; Jacob et al., 1996, 1997; Alonso et al., 1997, Cox and Deshusses, 1999, Okkerse et al., 1999) and the retention of inert suspended fine particles (as a matter of fact, wastewaters contain significant amounts of colloidal and particulate matter in addition to soluble substances) (Lowe, 1984; Bouwer, 1987; Drury et al., 1993; Jacob et al., 1996, 1997; Sheikholeslami, 1999) which narrows the free space for two-phase flow. The simultaneous overgrowth of attached biomass and deep-bed filtration of suspended fine particles lead to the progressive diminution of porosity and obstruction of the bed and are accompanied with an increase in pressure drop and flow channeling. Moreover, the excessive accumulation of fixed biomass leads to a progressive decrease of biofilm specific activity associated with substrate mass-transfer limitation (Alves et al., 1999). To prevent this problem, it is important to conserve a very thin and active biofilm rather than a thick and less effective biological fixed film. For maintaining acceptable operating cycles, the units require periodic backwashing and/or shutdowns for removing the excess biomass and specific solid deposits that have progressively built up across the pristine porous layer.

Several investigators in the past have attempted to theoretically describe the transient behavior of biomass accumulation (Deshusses et al., 1995; Alonso et al., 1997, 1998; Okkerse et al., 1999) and the biological clogging in trickle-bed bioreactors for waste-gas and wastewater treatment (Iliuta and Larachi, 2004a; Iliuta et al., 2004). On the other side, in recent years some authors have attempted to model single/two-phase flow and space-time evolution of the deposition of inert fines via deep-bed filtration (physical plugging) in fixed-bed reactors for non-biological applications, especially in the petroleum refining industry (Ortiz-Arroyo et al., 2002; Iliuta et al., 2003; Iliuta and Larachi, 2004b; Ortiz-Arroyo and Larachi, 2005).

In contrast, the literature still remains short about the complex hydrodynamics, physical and microbiological phenomena involved in the simultaneous *biological clogging* and *physical plugging* of trickle-bed bioreactors for aerobic wastewater treatment despite the critical operational problems of excessive biomass formation and retention of suspended fine particles. There is a lack of descriptive and quantitative reactor-scale models which can be used for predicting the fate of trickle bed hydrodynamics under biological clogging and physical plugging conditions and for planning strategies for minimizing the problem of clogging/plugging. Therefore, it is vital to gain new fundamental knowledge by tackling the complex hydrodynamics, physical and microbiological phenomena involved in the clogging/plugging of trickle beds due to the formation of excessive amount of biomass and the retention of suspended fine particles.

In this work, we propose to develop, based on the adaptation of the macroscopic *volume-average* form of the transport equations for multiphase systems a two-fluid two-dimensional transient model to quantify and understand the two-phase flow and the space-time evolution of simultaneous *biological clogging* and *physical plugging* in trickle-bed bioreactors for aerobic wastewater treatment. The general two-fluid model is based on the volume-average mass and momentum balance equations for the gas and liquid phases and continuity equation for the solid phase, the species balance equation for the fine particles, simultaneous transport and consumption of substrate and oxygen within the biofilm and solid particle, respectively the volume-average species balance equations for the liquid and gas phases. The model hypothesizes that physical plugging occurs via mono-layer deep-bed filtration mechanisms and biological clogging is induced by the formation of an excessive amount of biomass. The model incorporates physical effects of porosity and effective specific surface-area changes due to the capture of fine particles and biomass accumulation, the effects of biomass loss (via biomass decay and physical shearing), inertial effects of phases, and coupling effects between the filtration parameters and the interfacial momentum exchange force terms. Mono-layer deposition mechanisms are accounted for by including the appropriate filter coefficient expressions. Phenol biodegradation by *Pseudomonas putida* as the predominant species immobilized on activated carbon was chosen as a case study to illustrate the incidence of biomass accumulation on bioreactor hydrodynamics.

This contribution is a continuation of our endeavor in developing mathematical models for the description of biological clogging (Iliuta and Larachi, 2004a; Iliuta et al., 2004) or physical plugging via deep-bed filtration (Iliuta et al., 2003; Iliuta and Larachi, 2004b) in fixed bed reactors. The class of two-fluid transient models for the description of two-phase flow and space-time evolution of clogging/plugging has been upgraded by introducing a general model which describes *simultaneous biological clogging* and *physical plugging*.

2. Mathematical model development

Co-current downward gas–liquid *trickle flow* through a porous medium of uniform initial porosity and monodisperse particles is considered (Fig. 1a). At the reactor scale, the two-phase flow is assumed annular, separated

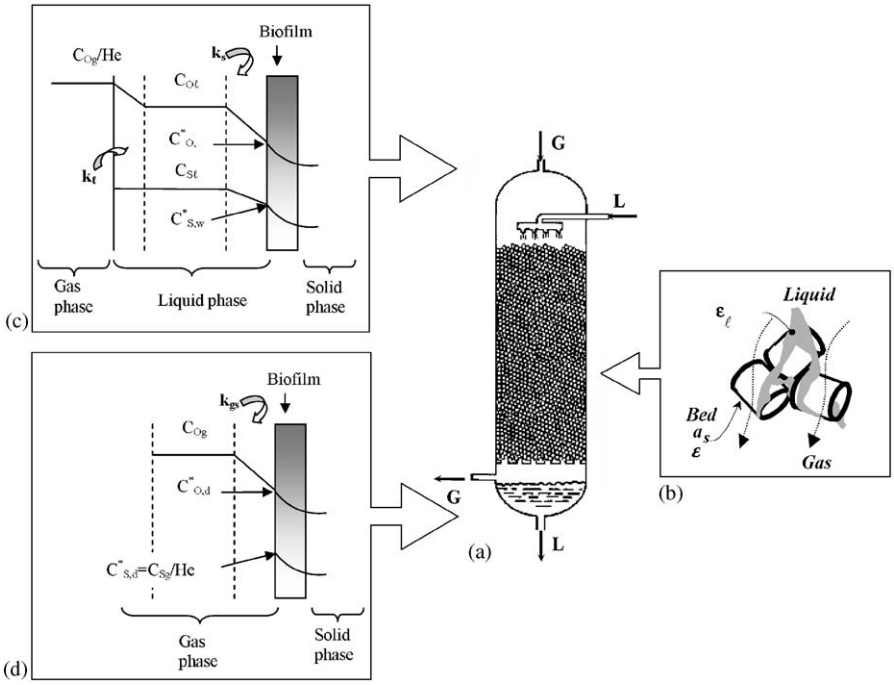

Fig. 1. Sketch of trickle bed bioreactor (a) and local scale representation of the two-phase flow (b). Sketch showing the resistances involved in the G/L reaction on the biofilm when the external surface area of the biocatalyst particle is completely wetted (c) and the external surface area of the biocatalyst particle is completely dry (d).

and unidirectional with both flowing fluids viscous Newtonian, whereas according to the spatial coordinate at the collecting particle scale, species diffusion (oxygen and substrate) occurs in spherical symmetry in biofilm and within the intraporous space of the collecting particle. The bioreactor inventory is viewed as a system of three interpenetrated continua: (i) a flowing (ideal) gas phase; (ii) a dilute *pseudohomogeneous* fluid phase consisting of the liquid and the seeding inert fine particles; (iii) and a stationary *pseudo-continuous* solid phase made up of the collecting particles (of the originally pristine porous medium), the captured fine particles and the biofilm consisting *inter alia* of microorganisms, extra-cellular polymeric substances and water. Each fluid phase is viewed as a continuum and the bioparticle surface is partially covered by a liquid film, i.e., partial wetting (Fig. 1b) and the gas flows in the remaining interstitial void. The properties of the liquid/fine suspension (density, viscosity, holdup) are equal to those of the embracing liquid (influent fines volume fraction $< 0.1‰$). Only the influent liquid was considered as a source for (the single-sized) fine particles. No bed plugging by the blocking or the sieving modes (Tien and Payatakes, 1979; Choo and Tien, 1995a) and no reentrainment of the deposited fine particles due to hydrodynamic drag forces are allowed in the present version of the model. The filtration mechanism to occur is of the mono-layer deep-bed filtration type and not of the cake filtration type (Narayan et al., 1997; Wang et al., 1999); in other words fine–fine attractive interactions within the fluid phase are assumed absent or at least small enough to preclude flocculation. The gas–liquid interface is impervious to the fine particles and the net sink in the fluid momentum balance due to fines mass transfer from fluid to the collector is neglected. The feed pollutant concentration is low so that bio-oxidation thermal effect is negligible and the bioreactor is isothermal. The phenol biodegradation by *P. putida* as the predominant species immobilized on activated carbon was considered.

The model is based on the volume average form of the transport equations for multiphase systems (Whitaker, 1973). The model equations consist of the conservation of volume, conservation of mass or continuity, conservation of momentum for the gas and fluid phases, continuity for the solid *stationary* phase (i.e., the fixed bed), the species balance for the fine particles undergoing displacement from the fluid phase to the solid phase and the species balance in the gas and liquid phases for both oxygen and substrate:

Conservation of volume:

$$\varepsilon_\ell + \varepsilon_g = \varepsilon. \tag{1}$$

Continuity for the gas and fluid phases:

$$\frac{\partial}{\partial t}(\varepsilon_g \rho_g) + \frac{\partial}{\partial z}(\varepsilon_g \rho_g u_g) = 0, \tag{2}$$

$$\frac{\partial}{\partial t}(\varepsilon_\ell \rho_\ell) + \frac{\partial}{\partial z}(\varepsilon_\ell \rho_\ell u_\ell) + \rho_f N = 0. \tag{3}$$

Continuity for the solid phase:

$$\frac{\partial}{\partial t}\left[(1-\varepsilon^o)\rho_s+\sigma\rho_f+\left(\varepsilon^o-\frac{\sigma}{1-\varepsilon_d}-\varepsilon\right)\rho_v\right] = \eta_G r_X a_s \delta_b - b a_s \delta_b \rho_v + \rho_f N. \quad (4)$$

Momentum balance equations for the gas and fluid phases:

$$\frac{\partial}{\partial t}(\rho_g \varepsilon_g u_g)+u_g\frac{\partial}{\partial z}(\rho_g\varepsilon_g u_g) = \varepsilon_g \mu_g^e \frac{\partial^2 u_g}{\partial z^2}-\varepsilon_g\frac{\partial P}{\partial z}+\varepsilon_g\rho_g g - F_{g\ell}-F_{gs}, \quad (5)$$

$$\frac{\partial}{\partial t}(\rho_\ell \varepsilon_\ell u_\ell)+u_\ell\frac{\partial}{\partial z}(\rho_\ell\varepsilon_\ell u_\ell) = \varepsilon_\ell \mu_\ell^e \frac{\partial^2 u_\ell}{\partial z^2}-\varepsilon_\ell\frac{\partial P}{\partial z}+\varepsilon_\ell\rho_\ell g + \frac{\varepsilon\eta_e-\varepsilon_\ell}{\varepsilon_g}[F_{g\ell}+F_{gs}]-F_{\ell s}. \quad (6)$$

Species balance for the fine particles:

$$\frac{\partial}{\partial t}(\varepsilon_\ell c)+u_\ell\frac{\partial}{\partial z}(\varepsilon_\ell c)=D_\ell\frac{\partial^2}{\partial z^2}(\varepsilon_\ell c)-N. \quad (7)$$

Species balance in fluid phase (axial dispersion model) for oxygen and substrate S (phenol: PhOH):

$$\frac{\partial}{\partial t}(C_{S\ell}\varepsilon_\ell)+u_\ell\frac{\partial}{\partial z}(C_{S\ell}\varepsilon_\ell) = D_\ell\frac{\partial^2}{\partial z^2}(C_{S\ell}\varepsilon_\ell)-\frac{r_X\rho_v}{Y_{X/S}}a_s\delta_b\eta_G, \quad (8)$$

$$\frac{\partial}{\partial t}(C_{O,\ell}\varepsilon_\ell)+u_\ell\frac{\partial}{\partial z}(C_{O,\ell}\varepsilon_\ell) = D_\ell\frac{\partial^2}{\partial z^2}(C_{O,\ell}\varepsilon_\ell)+k_\ell a(C_{Og}/He-C_{O\ell}) - \frac{r_x\rho_v}{Y_{X/O}}a_s\delta_b\eta_G. \quad (9)$$

Species balance in the gas phase (no axial dispersion in gas phase):

$$\frac{\partial}{\partial t}(C_{O,g}\varepsilon_g)+u_g\frac{\partial}{\partial z}(C_{O,g}\varepsilon_g) = -k_\ell a(C_{Og}/He-C_{O\ell})-D_{O,b}^{\text{eff}}\left.\frac{dC_{O,d}}{dr}\right|_{r=r_b} \times a_{sb}(1-\varepsilon)(1-\eta_e). \quad (10)$$

Filtration equation:

$$\frac{d\sigma}{dt}=N=\tfrac{3}{2}(1-\varepsilon^o)^{1/3}\frac{\eta}{d_p^o}cv_\ell. \quad (11)$$

Note that in the formulation of the momentum balance equations, the capillary pressure between the fluid and gas phases is neglected. The α-phase effective viscosity, μ_α^e, which arises from the combination of the viscous and the pseudo-turbulence stress tensors is formulated as proposed by Dankworth et al. (1990).

In the bioreactor model, the detachment of fine particles induced by hydrodynamic forces and by the colloidal forces was neglected. This is justified from the fact that Brownian and non-Brownian particles detachment by hydrodynamic mechanism is not possible in trickle-bed bioreactors for wastewater treatment due to the lower values of wall shear stress (knowing that the rate of detachment is proportional to the shear stress in excess of critical shear stress—Arulanandan et al., 1975; Khilar and Fogler, 1998). On the other side, Brownian particles release by colloidal forces is not important at lower values of liquid velocity (Ryan and Gschwend, 1994). However, the model takes into account the biomass loss which combines biomass decay and physical shearing.

Velocities at the inlet are specified in Dirichlet-type boundary conditions. At the outlet, an open boundary condition referred to as "outflow boundary condition" is used (Gresho and Sani, 1988). The liquid hold-up at the reactor inlet is calculated assuming $du_g/dz=du_\ell/dz=0$ and combining Eqs. (5) and (6) (Iliuta and Larachi, 2004a). Initial and boundary conditions for Eqs. (7)–(10) are:

$$t=0: \quad c=c^{\text{in}},\ C_{j\ell}=C_{j\ell}^{\text{in}},\ C_{Og}=C_{Og}^{\text{in}}, \text{ where } j=\text{O},\ \text{S}, \quad (12)$$

$$z=0: \quad u_\ell c^{\text{in}}=u_\ell c|_{z=0^+}-D_\ell\frac{\partial c}{\partial z}, \quad (13)$$

$$u_\ell C_{j\ell}^{\text{in}}=u_\ell C_{j\ell}|_{z=0^+}-D_\ell\frac{\partial C_{j\ell}}{\partial z}, \quad \text{where } j=\text{O},\ \text{S}, \quad (14)$$

$$C_{Og}=C_{Og}^{\text{in}}, \quad (15)$$

$$z=H: \quad \frac{dc}{dz}=0,\ \frac{\partial C_{j\ell}}{\partial z}=0, \quad \text{where } j=\text{O},\ \text{S}. \quad (16)$$

Solution of Eqs. (4), (8)–(10) requires knowledge of phenol and oxygen concentration profile within bioparticle (Figs. 1c, d). These concentration profiles are governed by the diffusional flux of phenol and oxygen within the bioparticle, the kinetics of consumption of both phenol and oxygen by cells constituting the biofilm, and the adsorption/desorption of phenol by the activated carbon particle. The simultaneous transport and reaction within the bioparticle is based on the following assumptions:

- Spherically-shaped and uniformly-sized bioparticles.
- Microorganisms uniformly distributed over particle surface forming uniform and stagnant biofilm.
- Homogeneous biofilm wherein phenol and oxygen diffusion obeys Fick's law.
- Various microbial species in the biofilm treated as a single *lumped* species so the biological parameters depicting pure culture activity can be employed to describe the lump metabolic activity.

- Phenol and oxygen are growth-limiting whereas all other nutrients are present in excess.
- Microbial immobilization onto particles entails no physiological change so that kinetics of cell growth and substrate degradation from suspended cell culture equally applies.
- Due to the inhibitory nature of phenol to the microorganisms (Tang et al., 1987), the Haldane equation was used to describe the growth kinetics of the culture.
- Effects of phenol and oxygen depletion due to adsorption on biofilm and solid particle are negligible; adsorption of oxygen by activated carbon is negligible.
- Particle internal wetting is complete, and reactants' diffusion inside particle occurs in liquid phase.

The mass balance equations for the biofilm expressed in spherical coordinates and the corresponding boundary and initial conditions are (the external surface area of the catalyst particle is completely wetted or completely dry):

$$\varepsilon_b \frac{\partial C_j}{\partial t} = \frac{1}{r^2}\frac{\partial}{\partial r}\left(r^2 D_{j,b}^{\text{eff}} \frac{\partial C_j}{\partial r}\right) - \frac{\mu \rho_v}{Y_{X/j}}, \quad j = \text{O, S} \tag{17}$$

in which ε_b is estimated from $(1-\rho_v/\rho_c)$ (Tang et al., 1987).

The simultaneous diffusion and adsorption of both phenol and oxygen within the activated carbon particles are given by

$$\varepsilon_p \frac{\partial C_j}{\partial t} + \rho_s \frac{\partial q_j}{\partial t} = \frac{1}{r^2}\frac{\partial}{\partial r}\left(r^2 D_{j,p}^{\text{eff}} \frac{\partial C_j}{\partial r}\right), \quad j = \text{O, S.} \tag{18}$$

The activated carbon particles with the biofilm completely removed were found to be reversible in the adsorption/desorption of phenol (Tang et al., 1987). The Langmuir equation was used to describe the adsorption/desorption isotherm in the following expression:

$$q_s = \frac{3825.3 C_{\text{S}}}{1 + 25.329 C_{\text{S}}}. \tag{19}$$

The corresponding boundary and initial conditions for Eqs. (19)–(20) are given as

$$r = 0: \quad \frac{\partial C_j}{\partial r} = 0, \tag{20}$$

$$r = r_p: \quad D_{j,b}^{\text{eff}} \left.\frac{\partial C_j}{\partial r}\right|_{r=r_p^+} = D_{j,p}^{\text{eff}} \left.\frac{\partial C_j}{\partial r}\right|_{r=r_p^-};$$
$$C_j|_{r_p^-} = C_j|_{r_p^+}, \tag{21}$$

$r = r_b$: the external surface area of the catalyst particle is completely wetted (to calculate η_ℓ)

$$D_{j,b}^{\text{eff}} \left.\frac{\partial C_{j,w}}{\partial r}\right|_{r=r_b} = k_{s,j}(C_{j,\ell} - C_{j,w}^*), \tag{22}$$

the external surface area of the catalyst particle is completely dry (to calculate η_g)

$$C_{\text{S},d}^* = C_{\text{S}\ell},$$
$$D_{\text{O},b}^{\text{eff}} \left.\frac{\partial C_{\text{O},d}}{\partial r}\right|_{r=r_b} = k_{gs,\text{O}}(\text{C}_{\text{O},g} - C_{\text{O},d}^* He), \tag{23}$$

$$t = 0: \quad C_j(r,0) = C_{j,\ell}^{\text{in}}. \tag{24}$$

2.1. Single-collector efficiency

The single-collector efficiency indicates the fraction of fine particles flowing toward a grain of media, or collector, that actually collides with the collector. In this work, the expression developed by Rajagopalan and Tien (1976) for application to mono-layer deep bed filtration was used to calculate the single-collector efficiency. Their analysis was based on the trajectory of a spherical fine particle in the vicinity of a spherical collector. The trajectory equation was developed by formulating a force balance for a suspended particle which included the effects due to the gravity, fluid drag, van der Waals interactions, and increased viscous resistance to particle motion near the collector surface. The flow in the porous medium was represented by Happel's sphere-in-cell model in which the packed bed is assumed to consist of spherical grains, each of which is encapsulated by a spherical liquid envelope. The diameter of the envelope is chosen such that the porosity of the unit formed by the grain and the liquid envelope is equal to the overall bed porosity. The contribution of Brownian diffusion to collection was based on an analytical solution of the convective diffusion equation for the Happel flow model (Rajagopalan and Tien, 1976). Combining this with the trajectory analysis yielded the following expression for the single-collector efficiency in terms of dimensionless parameters, N_L, N_R, N_G, and N_{Pe}, representing the mechanisms of particle–media interactions:

$$\eta = \frac{3}{2} A_s^o (1-\varepsilon^o)^{2/3} N_R^2 \times \left[\frac{2}{3} N_L^{1/8} N_R^{-1/8} + \frac{9}{4000} N_G^{6/5} N_R^{-12/5}\right] + 4(A_s^0)^{1/3}(1-\varepsilon^o)^{2/3} N_{Pe}^{-2/3}, \tag{25}$$

where

$$A_s^o = 2(1-p^5)/w, \quad p = (1-\varepsilon^o)^{1/3},$$
$$w = 2 - 3p + 3p^5 - 2p^6. \tag{26}$$

Here, N_R is the ratio of suspended particle size to collector size and indicates the importance of interception, N_G accounts for gravity effects, N_L reflects van der Waals interactions, and N_{Pe} expresses the role of Brownian diffusion.

2.2. Interfacial drag forces

The assumption of bed partial wetting entrains that the gas-phase drag will have contributions due to effects

located at the gas–liquid ($F_{g\ell}$) and gas–solid (F_{gs}) interfaces. Similarly, the resultant of the forces exerted on the liquid phase involves two components: (i) the drag force, $F_{\ell s}$, experienced by the liquid due to the shear stress nearby the liquid–solid boundary, (ii) and the gas–liquid interfacial drag due to the slip between fluids, $F_{g\ell}$.

Assuming trickle flow regime, the double slit model provides satisfactory approximations for the liquid–solid, gas–solid and gas–liquid drag forces (Iliuta et al., 2002):

$$F_{\ell s} = \eta_e \left\{ \frac{E_1}{36} C_w^2 \frac{a_{sb}^2 (1-\varepsilon)^2 \mu_\ell \eta_e}{\varepsilon_\ell^3} + \frac{E_2}{6} C_{wi} \frac{a_{sb}(1-\varepsilon)}{\varepsilon_\ell^3} \rho_\ell |v_\ell| \right\} v_\ell \varepsilon_\ell, \tag{27}$$

$$F_{gs} = (1-\eta_e) \left\{ \frac{E_1}{36} C_w^2 \frac{a_{sb}^2 (1-\varepsilon)^2 \mu_g}{\varepsilon^3} + \frac{E_2}{6} C_{wi} \frac{a_{sb}(1-\varepsilon)}{\varepsilon^3} \rho_g |v_g| \right\} v_g \varepsilon, \tag{28}$$

$$F_{g\ell} = \eta_e \left\{ \frac{E_1}{36} C_w^2 \frac{a_{sb}^2 (1-\varepsilon)^2 \mu_g}{(\varepsilon - \varepsilon_\ell/\eta_e)^2 \varepsilon_g} + \frac{E_2}{6} C_{wi} \frac{a_{sb}(1-\varepsilon)\rho_g}{(\varepsilon - \varepsilon_\ell/\eta_e)^2 \varepsilon_g} |v_g - (\varepsilon - \varepsilon_\ell/\eta_e) u^*| \right\} \times [v_g - (\varepsilon - \varepsilon_\ell/\eta_e) u^*] \varepsilon_g. \tag{29}$$

For an adaptation to the simultaneous physical and biological clogging context, these drag equations are recast as local functions of the local instantaneous values of the porosity and of the effective specific surface area, a_{sb}, of the bioparticle. This latter is used instead of the collector particle diameter because the effective specific surface area changes due to the biomass formation and retention of suspended fine particles. The specific area of the bioparticle was estimated at any time with the following relationship:

$$a_{sb} = \frac{6}{d_b}, \tag{30}$$

where d_b is the diameter of the bioparticle:

$$d_b = d_p(t) + 2\delta_b. \tag{31}$$

The bioparticle diameter was estimated using the simplified assumption that the biomass growth and fine particles deposition processes are superimposed. Since the microorganisms are uniformly distributed over the surface of activated carbon particles forming a uniform biofilm, the biofilm thickness was estimated at any time by means of the following relationship:

$$\delta_b = \frac{(\varepsilon^o - \varepsilon) - \frac{\sigma}{1-\varepsilon_d}}{a_s}. \tag{32}$$

The increase in the collector diameter due to the retention of the suspended fine particles was calculated as a function of the specific deposit assuming sphere-in-cell model configuration (Choo and Tien, 1995b):

$$d_p(t) = d_p^o \sqrt[3]{1 + \frac{\sigma}{(1-\varepsilon_d)(1-\varepsilon^o)}}. \tag{33}$$

2.3. Method of solution

In order to solve the system of partial differential equations, we discretized in space and solved the resulting set of ordinary differential equations. The spatial discretization is performed using the standard cell-centered finite difference scheme (at the reactor level) and the method of orthogonal collocation (at the solid particle and biofilm level). The number of collocation points specified for the biofim and activated carbon particle was restricted to 5. The GEAR integration method for stiff differential equations was employed to integrate the time derivatives. Simulations are carried out on a Pentium IV processor running at 2500 MHz. The relative error tolerance for the time integration process in the present simulations is set at 10^{-5} for each time step.

3. Results and discussion

3.1. Model parameters' estimation

The Ergun constants (E_1 and E_2), the volumetric gas–liquid ($k_\ell a$), liquid–solid (k_s) and gas–solid (k_{gs}) mass transfer coefficients, the liquid axial dispersion coefficient (D_ℓ), the external wetting efficiency (η_e), the diffusivities of phenol and oxygen within the biofilm, the shear/decay coefficient and kinetic parameters need to be specified. The Ergun single-phase flow parameters can be set either by measurements of single-phase pressure drops (Holub et al., 1992) or estimated from literature correlations (Iliuta et al., 1998). The volumetric gas–liquid mass transfer coefficients, liquid–solid mass transfer coefficient and wetting efficiency were estimated using recent literature correlations (Larachi et al., 2001, 2003). The gas-side mass transfer coefficient across the dry pellet region was calculated from the correlation of Goto and Smith (1975). The extent of back-mixing in the liquid phase is quantified in terms of an axial dispersion coefficient which is evaluated using a recent comprehensive Bodenstein number correlation (Piché et al., 2002). For the gas phase, previous experimental and theoretical investigations indicated marginal importance of axial mixing so that plug flow is assumed for this phase. The effective diffusion coefficient was evaluated assuming a tortuosity factor equal to 3. Diffusivities of phenol and oxygen within the biofilm were calculated using the correlation developed by Tang et al. (1987).

The model takes into account the biomass loss which combines biomass decay and physical shearing. Shear/decay rate coefficient was calculated using the model proposed by Alonso et al. (1997, 1998).

Table 1
Values of kinetic parameters

Kinetic parameter	Value
μ_{max}, h^{-1}	0.365
K_s, mg/L	10.948
K_i, mg/L	113.004
K_{ox}, mg/L	0.1
$K_{x/o}$, mg oxygen/mg phenol	0.354
$Y_{x/o}$, mg cell/mg phenol	0.496
Decay rate coefficient, b_d, h^{-1}	0.018
Default shear rate coefficient, b_{s0}, h^{-1}	2.08×10^{-4}

The kinetics parameters describing the growth of the microbial culture were determined by Tang and Fan (1987), see Table 1.

3.2. Model verification

There is no single work in the literature regarding experimental data for simultaneous biomass accumulation and fine particles deposition on two-phase flow trickle-bed bioreactors that could be used for validation of the proposed comprehensive model. However, the simplified variant of our approach based on the steady-state volume-averaged species balance equations at the reactor level (Eqs. (8)–(10)) coupled with the simultaneous transport and consumption of phenol and oxygen within the biofilm (Eq. (17)) and with the simultaneous diffusion of both phenol and oxygen and adsorption of phenol within the activated carbon particles (Eq. (18)) was compared to the experimental results obtained by Wisecarver and Fan (1989) and Hirata et al. (1986) in a gas–liquid–solid fluidized bed bioreactor with activated carbon particles ($d_p = 307\,\mu m$), respectively, with cement balls (d_p=388 and 623 μm) as the support particles. Table 2 shows an excellent agreement between the model predictions and experimental results. This agreement reflects the validity of the model over a wide range of biofilm thicknesses and ascertains the contribution of the biological clogging in the hydrodynamic model. In addition, in a previous work (Iliuta et al., 2003) we also validated the filtration model for two-phase flow coupled with fines deposition process in non-biological conditions ascertaining thus the role of physical plugging in the hydrodynamic model.

3.3. Simulations

The simultaneous biological clogging and physical plugging are sensitive to a diversity of biological and physical factors, e.g., microbial degradation rate, mechanical strength and morphology of developing biofilm (especially its density), packing characteristics, fine particle concentration, fines characteristics, etc. (Okkerse et al., 1999; Bouwer, 1987). To assess the impact of some phenomena occurring during simultaneous biological clogging and physical plugging, it is proposed to explore the potentialities of the developed model through simulations of different configurations by solving the above transport equations for trickle-bed bioreactors. The simulated conditions for phenol biodegradation are listed in Table 3. To illustrate the quantitative and qualitative features of clogging/plugging in trickle flow regime, the simulated results shown below are displayed (i) in terms of transient longitudinal profile snapshots of the local porosity, biofilm thickness and specific deposit, (ii) as well as in the form of transient pressure drop buildup at different values of the inlet phenol concentrations, total dry biomass in the biofilm, fine particles concentration and fine particles diameter.

Because phenol biodegradation rate is more noticeable at low inlet phenol concentration (at inlet phenol concentrations higher than 50 mg/l the cell growth rate decreases due to substrate inhibition, Iliuta, 1997), the following simulations were undertaken for these conditions. To treat wastewater containing high phenol concentration, either the

Table 2
Comparison of model predictions with experimental results (Wisecarver and Fan, 1989; Hirata et al., 1986) ($c^{in}_{O,\ell} = 2$ mg/l, $c^{in}_{O,g} = 275$ mg/l)

v_ℓ (m/s)	v_g (m/s)	$C^{in}_{S,\ell}$ (mg/l)	δ_b (μm)	ρ_v (mg/l)	Phenol conversion (experimental)	Phenol conversion (predicted)
000015	0.0076	242	41.2	78000	0.9967[a]	0.9950
000015	0.0076	256	59.8	81000	0.9984[a]	0.9962
000015	0.0076	220	123.3	47000	0.9964[a]	0.9995
000015	0.0076	245	31.6	74000	0.9976[a]	0.9985
000015	0.0076	192	28.5	73000	0.9995[a]	0.9982
000015	0.0076	240	29.1	73000	0.9996[a]	0.9982
00022	0.0015	97.1	346	15000	0.4222[b]	0.4156
00026	0.0081	117.5	181	30000	0.6025[b]	0.5981
00045	0.0015	96.0	302	16000	0.2274[b]	0.2212
00050	0.0025	51.7	308	16000	0.5354[b]	0.5280

[a]Data from Wisecarver and Fan (1989).
[b]Data from Hirata et al. (1986).

Table 3
Parameters used in simulations

Temperature, °C	25
Pressure, atm	1.0
Reactor diameter, m	0.051
Bed height, m	0.9
Diameter of support particle, m	0.003
Density of support particle, kg/m^3	1400
Internal porosity	0.575
External porosity	0.37
Superficial liquid velocity, m/s	0.0015
Superficial gas velocity, m/s	0.0283
Dry cell mass/wet cell volume, mg/l (Chiam and Harris, 1983)	670 000
Total dry biomass in the biofilm/ wet biofilm volume, mg/l	15 000–75 000
Henry's law constant	30
Diameter of kaolinite fine particles, μm	2–15
Density of kaolinite, kg/m^3	2000
Porosity of fines deposit layer (Tien, 1989; Gray et al., 2002)	0.8

residence time of wastewater in the reactor must be increased (by decreasing the wastewater influent flow rate or by increasing the reactor volume), or the wastewater must be diluted before feeding into the reactor (Tang and Fan, 1987). Also, because phenol biodegradation rate and biological clogging are more dramatic in the absence of biomass loss term (which combines biomass decay and physical shearing) (Fig. 2), the following simulations are undertaken under these conditions.

Figs. 3–5 show the history of the local porosity, biofilm thickness and the corresponding specific deposit at three bed depths in the bioreactor (near entrance, near mid-height and exit) for an inlet phenol concentration of 30 mg/l. In these figures (and in the next ones), $t=0$ represents the time corresponding to a biofilm thickness of 1 μm. Initially, uniformly-distributing shallow biofilm and specific solid deposit form across the whole bed depth. At later advanced times, biomass distribution and the extent of fines deposition become non-uniform (exception for Brownian particles when the extent of fines deposition is more homogeneous—Fig. 5b) and depend upon axial distance with a pronounced skewness towards bed entrance. Bed porosity decreases more in the bed entrance section because cell growth and fine particles deposition rates are the highest and biomass accumulation and specific solid deposit are the most prominent. Bed entrance section will therefore plug earlier than the lower sections of the bed. Towards the bioreactor exit, two factors become important in determining the decrease in biofilm thickness and solid deposit: (i) the cell growth slow down due to more severe substrate limitation (viz. phenol depletion), (ii) and fine particles deposition slow down due to the decrease of the fine particles concentration.

The relevant criterion to characterize and quantify the clogging/plugging is the bed pressure drop. Fig. 6 shows the effect of the fines feed concentration on the $\Delta P/\Delta P^o$ ratio

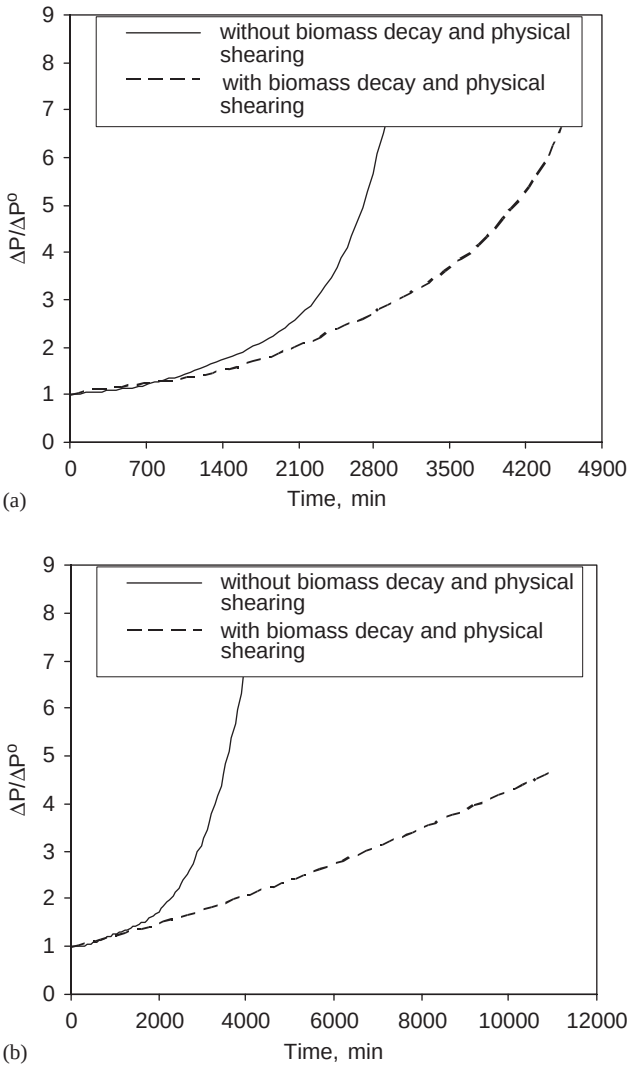

Fig. 2. Pressure drop ratio versus time in the presence or absence of biomass loss ($C^{in}_{S,\ell}=30$ mg/l, $C^{in}_{O,g}=275$ mg/l, $\rho_v=75\,000$mg/l, $d_f=10$ μm, $\Delta P^o=172.0$ Pa): (a) $c^{in}=0.05$ kg/m^3; (b) $c^{in}=0.01$ kg/m^3.

(where ΔP^o is the two-phase pressure drop for the clean bed under otherwise identical conditions). According to Eq. (11), higher fines concentrations give rise to higher filtration rates and consequently higher overall specific deposits (Fig. 7). As a result, the bed porosity decreases (physical plugging) and two-phase pressure drop increases. Fig. 8 shows the variation of the $\Delta P/\Delta P^o$ ratio with the inlet phenol concentration. With the increase of inlet phenol concentration, both the cell growth rate (Wisecarver and Fan, 1989; Iliuta, 1997) and the biomass accumulation increase yielding higher biofilm thickness. As a result, the bed porosity decreases (biological plugging) and two-phase pressure drop increases.

So, the key change resulting from biomass accumulation and fine particles deposition in the bed involves the effective porosity of the bed, and therefore the increase of two phase pressure drop is the result of the decrease in the

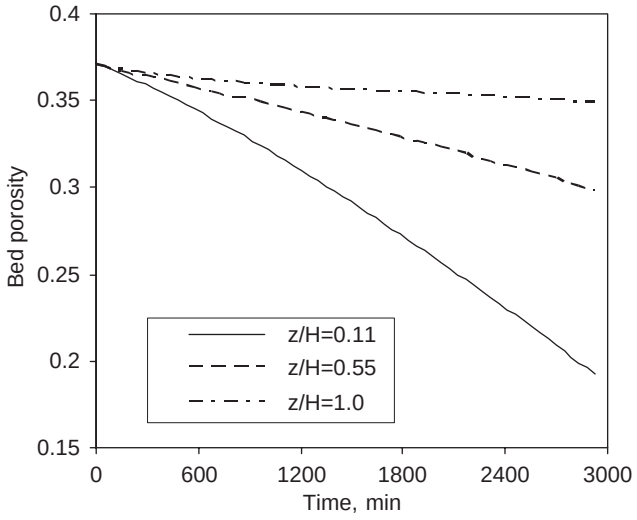

Fig. 3. Variation of the bed porosity with the dimensionless axial distance and the time ($C^{in}_{S,\ell} = 30$ mg/l, $C^{in}_{O,g} = 275$ mg/l, $\rho_v = 75\,000$ mg/l, $c^{in} = 0.05$ kg/m^3, $d_f = 10$ μm).

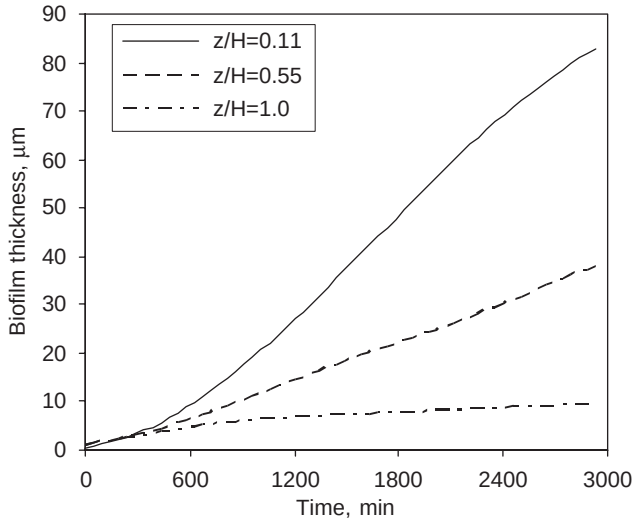

Fig. 4. Variation of the biofilm thickness with the dimensionless axial distance and the time ($C^{in}_{S,\ell} = 30$ mg/l, $C^{in}_{O,g} = 275$ mg/l, $\rho_v = 75\,000$ mg/l, $c^{in} = 0.05$ kg/m^3, $d_f = 10$ μm).

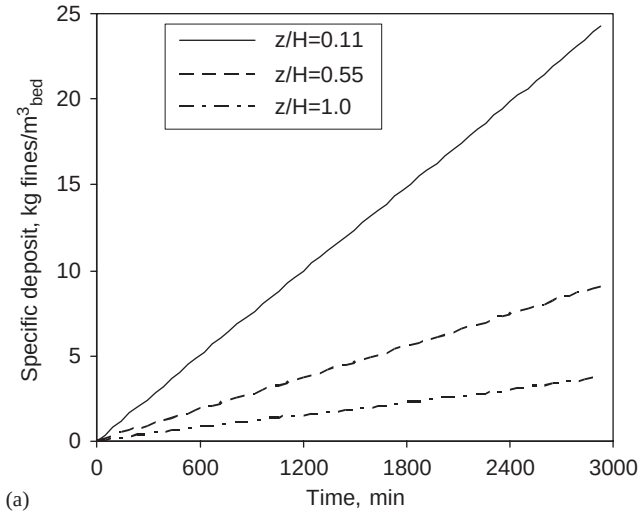

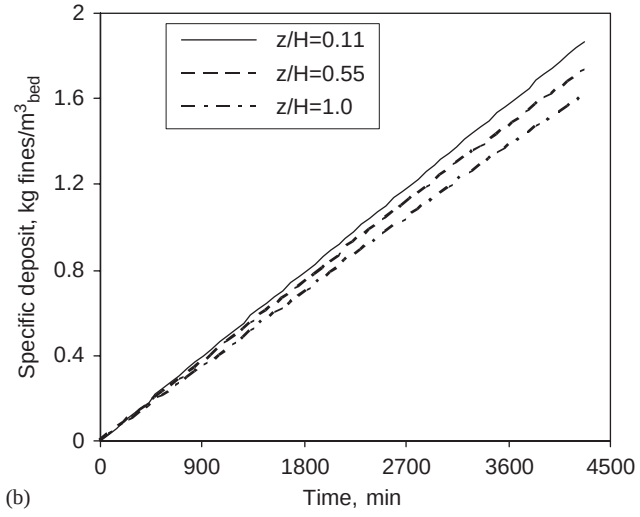

Fig. 5. Variation of the specific deposit with the dimensionless axial distance and the time ($C^{in}_{S,\ell} = 30$ mg/l, $C^{in}_{O,g} = 275$ mg/l, $\rho_v = 75\,000$ mg/l): (a) $c^{in} = 0.05$ kg/m^3, $d_f = 10$ μm; (b) $c^{in} = 0.03$ kg/m^3, $d_f = 2$ μm.

available free space. Consequently, the major change resulting from biomass accumulation and fines deposition in the bed involves the bed porosity, and therefore the pressure drop rise is mainly ascribed to a loss in available free space for gas and liquid flow.

Fig. 9 shows the effect of the fine particles diameter on the $\Delta P/\Delta P^o$ ratio. At higher fine particles diameter, the interception dimensionless group is higher and the filtration rate is higher yielding higher overall specific deposits (Fig. 10) at the same filtration time. As a result, the bed porosity decreases and the two-phase pressure drop increases. The deposition of larger fine particles promotes more confined physical plugging in the entrance region. This results in a more pronounced reduction in bed porosity in this section of the bioreactor bed (Fig. 5b). On the other side, with smaller diameter fines (Brownian particles) the extent of fines deposition is more homogeneous (Fig. 5b) and physical plugging spreads out more uniformly along the bed (Gray et al., 2002; Iliuta and Larachi, 2004b).

Fig. 11 depicts the effect of specific total dry biomass in the biofilm (ρ_v) on $\Delta P/\Delta P^o$ ratio assuming that the liquid phase contains 0.03 kg/m^3 fine particles. The decrease in the value of total dry biomass in the biofilm causes an increase in biofilm thickness and a lower bed porosity which translate into higher build-up in two-phase pressure drop ratio. Variation of biofilm thickness with biofilm dry density has been reported by several investigators (Hoehn and Ray, 1973; Timmermans and van Haute, 1984, Tang et al., 1987, Tang and Fan, 1987).

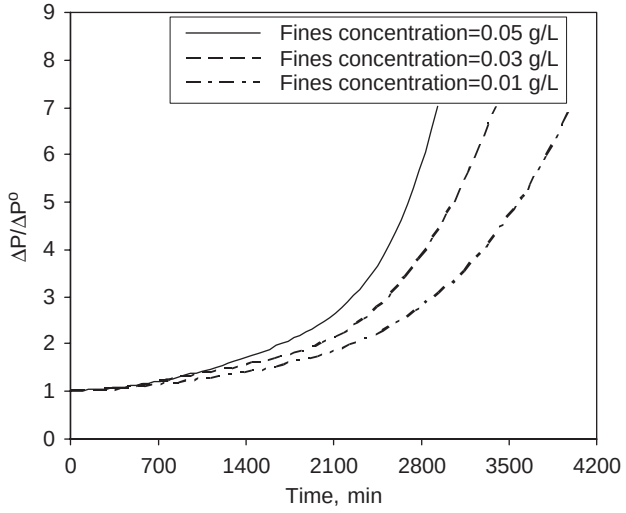

Fig. 6. Two-phase pressure drop ratio versus time at different values of fine particles concentration ($C^{\text{in}}_{\text{S},\ell}$=30 mg/l, $C^{\text{in}}_{\text{O},g}$=275 mg/l, ρ_v=75 000 mg/l, $d_f = 10\,\mu\text{m}$, $\Delta P^o = 172.0$ Pa).

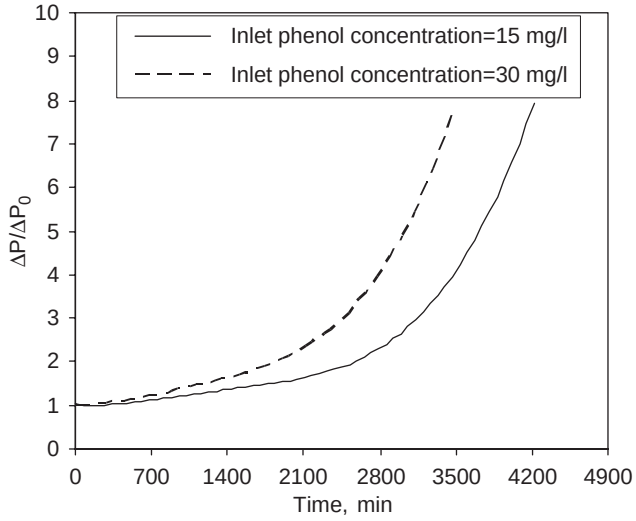

Fig. 8. Two-phase pressure drop ratio versus time at different values of inlet phenol concentration ($C^{\text{in}}_{\text{O},g}$=275 mg/l, ρ_v=75 000 mg/l, c^{in}=0.03 kg/m^3, $d_f = 10\,\mu\text{m}$, $\Delta P^o = 172.0$ Pa).

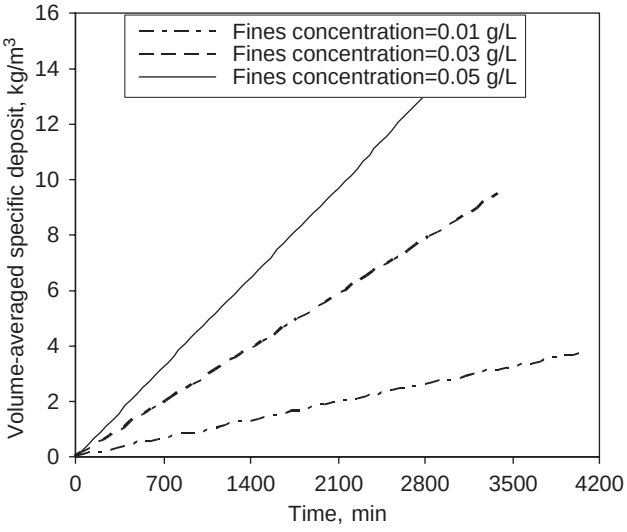

Fig. 7. Volume-averaged specific deposit versus time at different values of fine particles concentration ($C^{\text{in}}_{\text{S},\ell} = 30$ mg/l, $C^{\text{in}}_{\text{O},g} = 275$ mg/l, $\rho_v = 75\,000$ mg/l, $d_f = 10\,\mu\text{m}$).

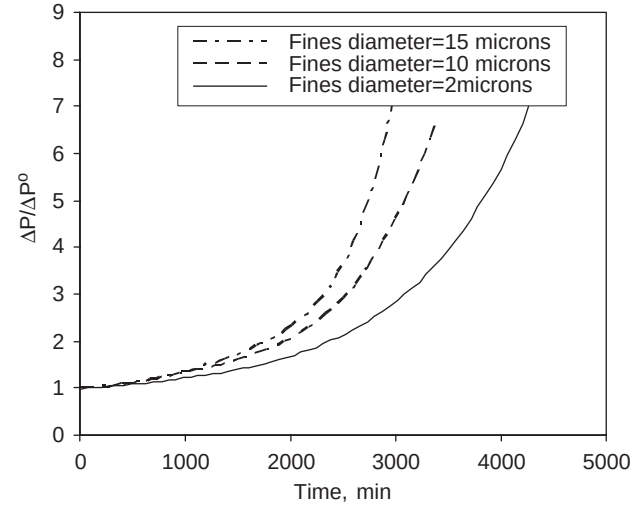

Fig. 9. Two-phase pressure drop ratio versus time at different values of fine particles diameter ($C^{\text{in}}_{\text{S},\ell}$=30 mg/l, $C^{\text{in}}_{\text{O},g}$=275 mg/l, ρ_v=75 000 mg/l, $c^{\text{in}} = 0.03$ kg/m^3, $\Delta P^o = 172.0$ Pa).

4. Conclusion

Removal of organic compounds from wastewater in trickle-bed bioreactors results in clogging due to biomass growth and plugging due to inert fine particles deposition. Excessive biomass formation and fine particles deposition lead to the progressive diminution of porosity and obstruction of the bed that is accompanied with pressure drop build-up and flow channeling. A 2-D transient two-fluid dynamic model based on the macroscopic volume-averaged mass and momentum balance equations, continuity equation for the solid phase, the species balance equation for the fine particles and volume-averaged species balance equations at the reactor level coupled with the simultaneous transport and consumption of phenol and oxygen within the biofilm and with the simultaneous diffusion of both phenol and oxygen and adsorption of phenol within the activated carbon particles was proposed for the description of two-phase flow and space-time evolution of biological clogging and physical plugging in trickle flow bioreactors. The model hypothesizes that physical plugging occurs via mono-layer deep-bed filtration mechanisms and biological clogging is induced by the formation of an excessive amount of biomass. The phenol biodegradation by *Pseudomonas putida* as the predominant species immobilized on activated

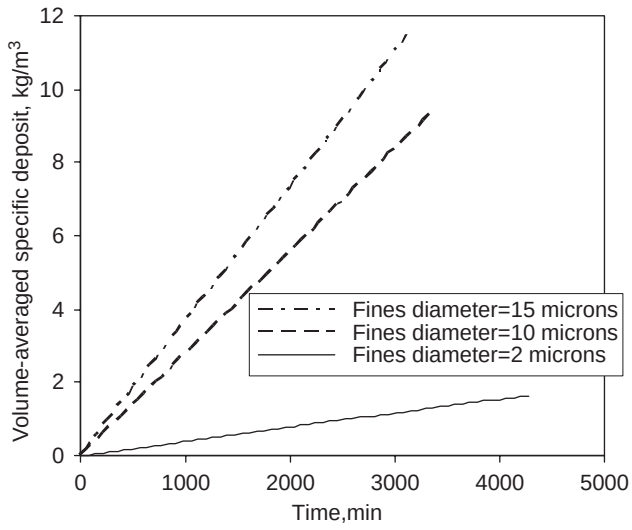

Fig. 10. Volume-averaged specific deposit versus time at different values of fine particles diameter ($C^{\text{in}}_{\text{S},\ell}$=30 mg/l, $C^{\text{in}}_{\text{O},g}$=275 mg/l, ρ_v=75 000 mg/l, $c^{\text{in}} = 0.03\,\text{kg/m}^3$).

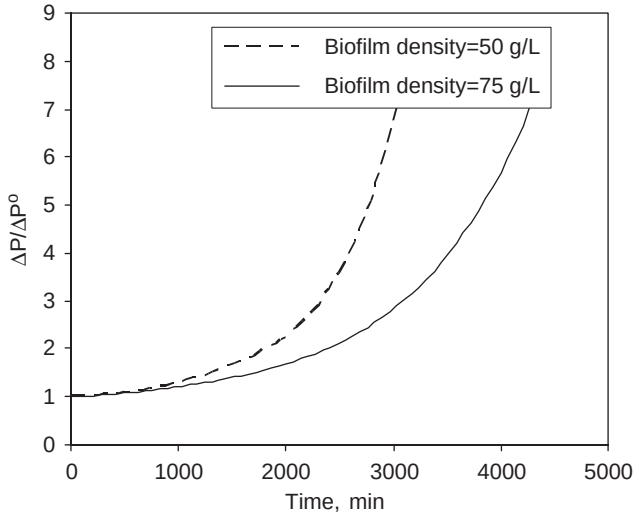

Fig. 11. Two-phase pressure drop ratio versus time at different values of total dry biomass in the biofilm ($C^{\text{in}}_{\text{S},\ell} = 30\,\text{mg/l}$, $C^{\text{in}}_{\text{O},g} = 275\,\text{mg/l}$, $c^{\text{in}} = 0.03\,\text{kg/m}^3$, $d_f = 2\,\mu\text{m}$, $\Delta P^o = 172.0\,\text{Pa}$).

carbon was chosen as a case study illustrating the consequences of formation of excessive amount of biomass. The impact of the formation of an excessive amount of biomass and the retention of suspended fine particles was evaluated in terms of pressure drop rise as a function of time, as well as in terms of clogging/plugging patterns, e.g., local porosity, solid deposit and biofilm thickness versus bed depth.

Notation

a_s specific area of the bed after fine particles deposition, $a_s = \frac{6}{d_p(t)}\left[1 - \varepsilon^o + \frac{\sigma}{1-\varepsilon_d}\right]$

a_s^o specific area of the packing (surface of the particles/volume of the bed), m^2/m^3

a_{sb} specific area of the bioparticle, $\text{m}^2/\text{m}^3_{\text{bioparticle}}$

b shear/decay rate coefficient, $b = b_d + b_{s0}\left(\frac{\varepsilon^0}{\varepsilon}\right)^2$, s^{-1}

c fine particles volumetric concentration (liquid volume basis)

C_j concentration of component j (j = O, S), kg/m^3

$C_{j,d}$ concentration of component j in the biofilm when the external surface area of the biocatalyst particle is completely dry (j = O, S), kg/m^3

$C_{j,w}$ concentration of component j in the biofilm when the external surface area of the biocatalyst particle is completely wetted (j = O, S), kg/m^3

C_w, C_{wi} wall correction functions (Liu et al., 1994)

d_b bioparticle diameter, m

d_f fine particle diameter, m

d_p effective particle diameter, m

D_{BM} Brownian diffusion coefficient, $D_{\text{BM}} = \frac{2k_B T}{6\pi\mu_\ell d_f}$

D_j molecular diffusivity of component j, m^2/s

D_j^{eff} effective diffusivity of component j, m^2/s

D_ℓ liquid axial dispersion coefficient, m^2/s

E_1, E_2 Ergun constants, dimensionless

$F_{g\lambda}$ gas–liquid drag force, N/m^3

F_{gs} gas–solid drag force, N/m^3

$F\lambda_s$ liquid–solid drag force, N/m^3

g gravitational acceleration, m/s^2

H bed height, m

Ha Hamaker constant, J

He Henry constant

k_B Boltzmann's constant, J/K

k_{gs} gas–solid mass transfer coefficient, m/s

k_i inhibition constant, kg/m^3

$k_\ell a$ volumetric liquid-side mass transfer coefficient, s^{-1}

K_{ox} saturation constant of oxygen, kg/m^3

k_s liquid–solid mass transfer coefficient, m/s

K_{S} saturation constant of phenol, kg/m^3

N filtration rate (reactor volume basis), s^{-1}

N_G gravitational dimensionless group, $N_G = \frac{(\rho_f - \rho_\ell)d_f^2 g}{18\pi\mu_\ell v_\ell}$

N_L London–van der Waals dimensionless group, $N_L = \frac{4Ha}{9\pi\mu_\ell d_f^2 v_\ell}$

N_{Pe} Brownian diffusion group, $N_{Pe} = \frac{d_p(t)v_\ell}{D_{\text{BM}}}$

N_R interception dimensionless group, $N_R = \frac{d_f}{d_p^o}$

P pressure, Pa

q_j amount of component j adsorbed per unit weight of activated carbon

r radial position within bioparticle, m

r_b radius of the bioparticle, m
r_p radius of the support particle (m)
r_X cell growth rate, $r_X = \mu\rho_v$, $\mathrm{kg/m^3_{biofilm}s}$
t time, s
T temperature, K
u_α average interstitial velocity of α-fluid, m/s
u^* interfacial velocity, m/s
v_α α-phase superficial velocity, m/s
$Y_{X/O}$ yield coefficient, kg biomass/kg oxygen
$Y_{X/S}$ yield coefficient, kg biomass/kg phenol
z axial coordinate, m

Greek letters

δ_b biofilm thickness, m
ε bed porosity, dimensionless
ε_b porosity of biofilm, dimensionless
ε_d fines deposit porosity
ε_g gas holdup, dimensionless
ε_ℓ liquid holdup, dimensionless
ε_p particle porosity, dimensionless
η collector efficiency
η_e external wetting efficiency
η_g effectiveness factor for a completely dry particle
η_G overall effectiveness factor, dimensionless
η_ℓ effectiveness factor for a fully wetted particle
μ specific growth rate, $\mu = \dfrac{\mu_{\max} C_S}{K_s + C_S + C_S^2/K_i} \dfrac{C_O}{K_{ox} + C_O}$, $\mathrm{s^{-1}}$
$\mu_{\max}$ maximum specific growth rate, $\mathrm{s^{-1}}$
$\mu\alpha$ α phase dynamic viscosity, $\mathrm{kg/m \cdot s}$
μ^e_α α phase effective viscosity (combination of bulk and shear terms), $\mathrm{kg/m \cdot s}$
ρ_c dry cell mass/wet cell volume, $\mathrm{kg/m^3}$
ρ_v total dry biomass in the biofilm, $\mathrm{kg/m^3}$
$\rho\alpha$ density of α phase, $\mathrm{kg/m^3}$
σ specific deposit (reactor volume basis), $\sigma = (\varepsilon^o - \varepsilon - a_s\delta_b)(1 - \varepsilon_d)$
σ volume-averaged specific deposit, $\langle\sigma\rangle = H^{-1}\int_0^H \sigma(t)\,\mathrm{d}z$

Subscripts/superscripts

b biofilm
g gas
f fine particle
in inlet
ℓ liquid
o clean bed state
O oxygen
s solid phase
S phenol
$*$ on biocatalyst surface

References

Alonso, C., Suidan, M.T., Sorial, G.A., Smith, F.L., Biswas, P., Smith, P.J., Brenner, R.C., 1997. Gas treatment in trickle-bed biofilters: biomass, how much is enough? Biotechnology and Bioengineering 54, 583–594.

Alonso, C., Suidan, M.T., Kim, B.R., Kim, B.I., 1998. Dynamic mathematical model for the biodegradation of VOCs in a biofilter: biomass accumulation study. Environmental Science and Technology 32, 3118–3123.

Alves, M.M., Pereira, M.A., Novais, J.M., Fernandez-Polanco, F., Mota, M., 1999. A new device to select microcarriers for biomass immobilization: application to an anaerobic consortium. Water Environment Research 71, 209–217.

Arulanandan, K., Longanathan, P., Krone, R.B., 1975. Pore and eroding fluid influences on surface erosion of soil. Journal of Geotechnical Engineering Division - ASCE 101, 51–65.

Benthack, C., Srinivasan, B., Bonvin, D., 2001. An optimal operating strategy for fixed-bed bioreactors used in wastewater treatment. Biotechnology and Bioengineering 72, 34–40.

Bouwer, E.J., 1987. Theoretical investigation of particle deposition in biofilm systems. Water Research 21, 1489–1498.

Chaudhry, M.A., Bed, S.A., 1998. A review on the mathematical modeling of biofilm processes: advances in fundamentals of biofilm modeling. Chemical Engineering and Technology 21, 701–710.

Chiam, H.F., Harris, I.J., 1983. Application of a noninhibitory growth model to predict the transient response in a chemostat. Biotechnology and Bioengineering 25, 1613–1623.

Choo, C.-U., Tien, C., 1995a. Simulation of hydrosol deposition in granular media. A.I.Ch.E. Journal 41, 1426–1436.

Choo, C.-U., Tien, C., 1995b. Analysis of the transient behavior of deep-bed filtration. Journal of Colloid and Interface Science 169, 13–33.

Cox, H.H.J., Deshusses, M.A., 1999. Biomass control in waste air biotrickling filters by protozoan predation. Biotechnology and Bioengineering 62, 216–224.

Dankworth, D.C., Kevrekidis, I.G., Sundaresan, S., 1990. Dynamics of pulsing in trickle beds. A.I.Ch.E. Journal 36, 605–621.

Deshusses, M.A., Hamer, G., Dunn, I.J., 1995. Behavior of biofilters for waste air biotreatment. 1. Dynamic model development. Environmental Science and Technology 29, 1048–1058.

Drury, W.J., Stewart, P.S., Characklis, W.G., 1993. Transport of 1-μm latex particles in *Pseudomonas aeruginosa* biofilms. Biotechnology and Bioengineering 42, 111–117.

Goto, S., Smith, J.M., 1975. Trickle-bed reactors performance, Part-1: holdup and mass transfer effects. A.I.Ch.E. Journal 21, 706–713.

Gray, M.R., Srinivasan, N., Masliyah, J.H., 2002. Pressure buildup in gas–liquid flow through packed beds due to deposition of fine particles. Canadian Journal of Chemical Engineering 80, 346–354.

Gresho, P.M., Sani, R.L., 1988. Incompressible flow and the finite element method. Advection–Diffusion and Isothermal Laminar Flow, Wiley, Chichester, UK.

Hirata, A., Hosaka, Y., Umezawa, H., 1986. Biological treatment of water and wastewater in three-phase fluidized bed. Proceedings of the Third World Congress in Chemical Engineering, vol. III, Tokyo, p. 556.

Hoehn, R.G., Ray, A.D., 1973. Effects of thickness on bacterial film. Journal of Water Pollution Control Federation 45, 2302–2309.

Holub, R.A., Dudukovic, M.P., Ramachandran, P.A., 1992. A phenomenological model of pressure drop, liquid holdup and flow regime transition in gas–liquid trickle flow. Chemical Engineering Science 47, 2343–2351.

Iliuta, I., 1997. Performance of fixed bed reactors with two-phase upflow and downflow. Journal of Chemical Technology and Biotechnology 68, 47–56.

Iliuta, I., Larachi, F., 2004a. Biomass accumulation and clogging in trickle-bed bioreactors. A.I.Ch.E. Journal 50, 2541–2551.

Iliuta, I., Larachi, F., 2004b. Onset of pulsing in gas–liquid trickle bed filtration. Chemical Engineering Science 59, 1199–1211.

Iliuta, I., Larachi, F., Grandjean, B.P.A., 1998. Pressure drop and liquid hold-up in trickle flow reactors: improved Ergun constants and slip correlations for the slit model. Industrial and Engineering Chemistry Research 37, 4542–4550.

Iliuta, I., Grandjean, B.P.A., Larachi, F., 2002. New mechanistic film model for pressure drop and liquid holdup in trickle flow reactors. Chemical Engineering Science 57, 3359–3371.

Iliuta, I., Larachi, F., Grandjean, B.P.A., 2003. Fines deposition dynamics in trickle flow reactors. A.I.Ch.E. Journal 49, 485–495.

Iliuta, I., Iliuta, M.C., Larachi, F., 2004. Hydrodynamics modeling of bioclogging in waste gas treating trickle bed reactors. Industrial and Engineering Chemistry Research, in press.

Jacob, J., Pingaud, H., Le Lann, J.-L., Bourrel, S., Babary, J.P., Capdeville, B., 1996. Dynamic simulation of biofilters. Simulation Practice and Theory 4, 335–348.

Jacob, J., Le Lann, J.-M., Pingaud, H., Capdeville, B., 1997. A generalized approach for dynamic modelling and simulation of biofilters: application to waste-water denitrification. Chemical Engineering Journal 65, 133–143.

Khilar, K.C., Fogler, H.S., 1998. Migration of Fines in Porous Media, Kluwer Academic Publishers, Dordrecht, Boston, London.

Larachi, F., Belfares, L., Grandjean, B.P.A., 2001. Prediction of liquid–solid wetting efficiency in trickle flow reactors. International Communications in Heat and Mass Transfer 28, 595–602.

Larachi, F., Belfares, L., Iliuta, I., Grandjean, B.P.A., 2003. Heat and mass transfer in co-current gas–liquid packed beds analysis, recommendations and new correlations. Industrial and Engineering Chemistry Research 42, 222–242.

van Lith, C.P.M., Ottengraf, S.P.P., Diks, R.M.M., 1994. The control of a biotrickling filter. VDI Berichte 1104, 169–180.

Liu, S., Afacan, A., Masliyah, J.H., 1994. Steady incompressible laminar flow in porous media. Chemical Engineering Science 21, 3565–3576.

Lowe, M.J., 1984. Biological-particulate fouling interactions. In: Proceedings First National UK Heat Transfer Conference, Leeds, UK, pp. 391–400.

Narayan, R., Coury, J.R., Masliyah, J.H., Gray, M.R., 1997. Particle capture and plugging in packed-beds reactors. Industrial and Engineering Chemistry Research 36, 4620–4627.

Okkerse, W.J.H., Ottengraf, S.P.P., Osinga-Kuipers, B., Okkerse, M., 1999. Biomass accumulation and clogging in biotrickling filters for waste gas treatment. Evaluation of the dynamic model using dichloromethane as a model pollutant. Biotechnology and Bioengineering 63, 418–430.

Ortiz-Arroyo, A., Larachi, F., 2005. Lagrange–Euler–Euler CFD approach for modeling deep bed filtration in trickle flow reactors. Separation and Purification Technology 41, 155–172.

Ortiz-Arroyo, A., Larachi, F., Grandjean, B.P.A., Roy, S., 2002. CFD modeling and simulation of clogging in packed beds with non-aqueous media. A.I.Ch.E. Journal 48, 1596–1609.

Piché, S., Larachi, F., Iliuta, I., Grandjean, B.P.A., 2002. Improving predictions of liquid back-mixing in trickle-bed reactors using a neural network approach. Journal of Chemical Technology and Biotechnology 77, 989–998.

Pujol, R., Canler, J.P., Iwema, A., 1992. Biological aerated filters: an attractive and alternative biological process. Water Science and Technology 26, 693–702.

Rajagopalan, R., Tien, C., 1976. Trajectory analysis of deep-bed filtration with the sphere-in-cell porous media model. A.I.Ch.E. Journal 22, 523–533.

Ryan, J.N., Gschwend, P.M., 1994. Effects of ionic strength and flow rate on colloid release: relating kinetics to intersurface potential energy. Journal of Colloid and Interface Science 164, 21–34.

Sheikholeslami, R., 1999. Composite fouling—inorganic and biological: a review. Environmental Progress 18, 113–122.

Sorial, G.A., Smith, F.L., Suidan, M.T., Biswas, P., 1995. Evaluation of a trickle bed biofilter media for toluene removal. Journal of Air and Waste Management Association 45, 801–810.

Tang, W.-T., Fan, L.-S., 1987. Steady state phenol degradation in a draft-tube, gas–liquid–solid fluidized-bed bioreactor. A.I.Ch.E. Journal 33, 239–249.

Tang, W.-T., Wisecarver, K., Fan, L.-S., 1987. Dynamics of a draft tube gas–liquid–solid fluidized bed bioreactor for phenol degradation. Chemical Engineering Science 42, 2123–2134.

Tien, C., 1989. Granular Filtration of Aerosols and Hydrosols, Butterworths-Heinemann Series in Chemical Engineering, Boston.

Tien, C., Payatakes, A.C., 1979. Advances in deep bed filtration. A.I.Ch.E. Journal 25, 737–759.

Timmermans, P., van Haute, A., 1984. Influence of the type of organisms on the biomass hold-up in fluidized-bed reactor. Applied Microbiology and Biotechnology 19, 36–44.

Wang, S., Chung, K.H., Masliyah, J.H., Gray, M.R., 1999. Deposition of fine particles in packed beds at hydrotreating conditions: role of surface chemistry. Industrial and Engineering Chemistry Research 38, 4878–4888.

Weber, F.J., Hartmans, S., 1994. Toluene degradation in a trickle-bed reactor—prevention of clogging. VDI Berichte 1104, 161–168.

Weber, F.J., Hartmans, S., 1996. Prevention of clogging in a biological trickle-bed reactor removing toluene from contaminated air. Biotechnology and Bioengineering 50, 91–97.

Whitaker, S., 1973. The transport equations for multi-phase systems. Chemical Engineering Science 28, 139–147.

Wisecarver, K.D., Fan, L.-S., 1989. Biological phenol degradation in a gas–liquid–solid fluidized bed reactor. Biotechnology and Bioengineering 33, 1029–1038.